Journal of Modern Optics
Vol. 54, Nos. 2–3, 20 January–15 February 2007, 453–465

Single photon sources based upon single quantum dots in semiconductor microcavity pillars

J. A. TIMPSON*†, D. SANVITTO†, A. DARAEI†, P. S. S. GUIMARAES†, H. VINCK†, S. LAM†, D. M. WHITTAKER†, M. S. SKOLNICK†, A. M. FOX†, C. Y. HU‡, Y.-L. D. HO‡, R. GIBSON‡, J. G. RARITY‡, S. PELLEGRINI§, K. J. GORDON§, R. E. WARBURTON§, G. S. BULLER§, A. TAHRAOUI¶, P. W. FRY¶ and M. HOPKINSON¶

†Department of Physics and Astronomy, University of Sheffield, Sheffield S3 7RH, UK
‡Department of Electrical & Electronic Engineering, University of Bristol, Bristol BS8 1UB, UK
§School of Engineering and Physical Sciences, Heriot Watt University, Edinburgh, EH14 4AS, UK
¶Department of Electronic and Electrical Engineering, University of Sheffield, Sheffield S1 3JD, UK

(*Received 10 February 2006; in final form 3 May 2006*)

Semiconductor microcavity pillars with both circular and elliptical cross-section containing semiconductor quantum dots are shown to be good candidates for efficient single photon sources. Pillars with small diameters are shown to have exceptionally high quality factors and the reduction in the measured quality factor as the pillar diameter is reduced is shown to agree well with finite difference time domain simulation. These pillars exhibit a Purcell enhancement of the quantum dot emission when the dots are on-resonance with the cavity mode and strong photon antibunching. The use of the polarized modes of an elliptical micropillar allows the polarization of the emitted single photons to be selected.

1. Introduction

An efficient source of single photons would allow significant advances in the field of quantum information processing [1], most immediately in quantum key distribution [2]. Single photon sources have been demonstrated, for example, using single molecules [3], colour centres in diamond [4] and semiconductor quantum dots [5, 6]. One advantage of semiconductor quantum dots is their compatibility with the advanced processing techniques developed by the semiconductor industry, allowing them to be incorporated easily within microcavities, improving both the

*Corresponding author. Email: J.A.Timpson@sheffield.ac.uk

Journal of Modern Optics
ISSN 0950–0340 print/ISSN 1362–3044 online © 2007 Taylor & Francis
http://www.tandf.co.uk/journals
DOI: 10.1080/09500340600785055

quantum dot emission rate via the Purcell effect [7, 8] and the photon collection efficiency [7, 8].

In this paper we report small diameter microcavity pillars with exceptionally high quality factors. The Purcell enhancement factor (P_F) of the spontaneous emission of a quantum dot embedded within the microcavity is calculated to be very high, with $P_F > 70$ for a 1.5 μm diameter pillar. When the quantum dot emission energy is on-resonance with the cavity mode, the spontaneous emission rate is shown to be enhanced and, as required for a single photon source, the multi-photon emission probability is reduced to a very low level (in the case of a 0.6 μm diameter pillar the multi-photon emission is suppressed by at least a factor of 20 compared to a Poissonian source with the same intensity). Using the polarized modes of a micropillar with elliptical cross-section [9–11] the emission from a quantum dot can be tuned so that the emission has a degree of linear polarization in excess of 0.9. (Note that similar results have also been observed in certain designs of photonic crystal [12].)

Section 2 will describe the sample details and section 3 will describe the two experimental arrangements used in this work. Section 4 contains the experimental results, starting with the measured and simulated quality (Q) factors. The control of the polarization of the single photon sources in elliptical micropillars is then described followed by a discussion of quantum dot lifetimes. Finally, results demonstrating single photon generation in both circular and elliptical micropillars will be presented.

2. Sample details

The microcavity structure consists of a one wavelength thick GaAs cavity surrounded by 27 pairs of alternating $Al_{0.9}Ga_{0.1}As$/GaAs layers in the bottom distributed Bragg reflector (DBR) and 20 pairs in the top DBR. The cavity contains a single layer of low density InAs quantum dots positioned at the cavity antinode. The samples were grown by molecular beam epitaxy using *in situ* reflectivity monitoring.

The samples were processed using a combination of electron beam lithography (EBL) and inductively coupled plasma (ICP) etching. First, a 600 nm layer of SiO_2 was deposited, followed by an ~300 nm thick poly(methylmethacrylate) layer which was patterned using EBL. A 100 nm thick layer of aluminium was evaporated on the sample and the desired pattern transferred to this using lift-off to leave metal discs; these discs served as a mask allowing the SiO_2 to be etched using a CHF_3 based reactive ion etching. The metal discs were then chemically removed, leaving a SiO_2 mask. Pillars were then formed using a $SiCl_4/Cl_2$-based ICP. The SiO_2 layer facilitates the etching of high aspect ratio pillars and inhibits degradation of the side walls which would occur during the removal of the aluminium mask. A micrograph of a 1.5 μm diameter pillar is shown in the inset to figure 1. The smooth, nearly vertical side walls clearly show the high quality of the etching.

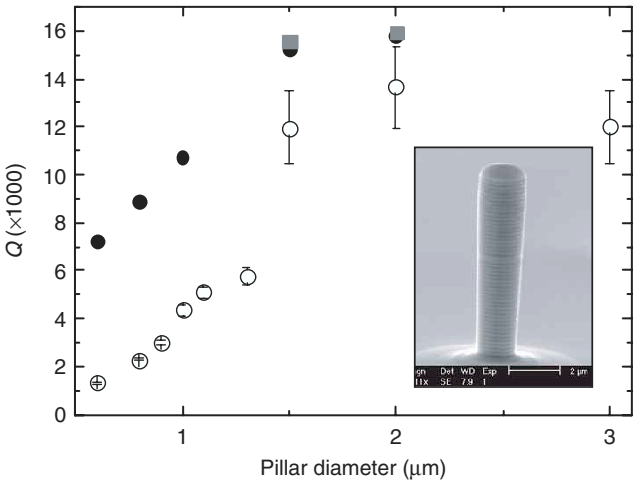

Figure 1. Quality factors for microcavity pillars with circular cross-sections. Hollow points show the measured Q factors, while solid black circular (solid grey square) points show Q factors predicted by FDTD simulations for micropillars with circular (square) cross-section. The inset shows an electron microscope image of a micropillar with circular cross-section and a diameter of 1.5 μm, measured at the cavity centre.

Each sample contained a series of micropillars with both circular and elliptical cross-sections, the circles ranging in diameter from 50 μm to 600 nm and the ellipses having major and minor axes ranging from 5 to 1.5 μm and 4 to 0.5 μm, respectively.

3. Experimental details

In this paper two different types of measurements are reported: continuous wave (cw) and time-resolved measurements. The experimental layout is shown in figure 2. To measure micropillar Q factors and the polarization of dot emission both on- and off-resonance with the cavity mode, the following arrangement was used. The sample was cooled to temperatures between 4.2 and 50 K in a liquid helium continuous flow cryostat. In the cryostat the sample was mounted close to a thin window allowing high resolution micro-photoluminescence (μPL) spectra to be measured. Excitation was provided by the 633 nm line from a He:Ne laser. A microscope objective with a numerical aperture of 0.5 focused the laser to a spot of diameter ~2 μm and collected the emitted PL emission which was then dispersed in a 0.75 m double spectrometer. Using high excitation power (~200 μW in a 2 μm diameter spot) the measured spectra show broadband emission from, for example, the tail of the wetting layer, modulated by the cavity mode. Under these conditions single dot emission was not resolved. Single dot emission was measured using low power excitation (~5 μW in a 2 μm diameter spot).

A similar apparatus was used for the time-resolved micro-photoluminescence (TRPL) experiments, except that the laser used was a picosecond mode-locked Ti:Sapphire laser with a pulse length of 3 ps, a repetition rate of 82 MHz and

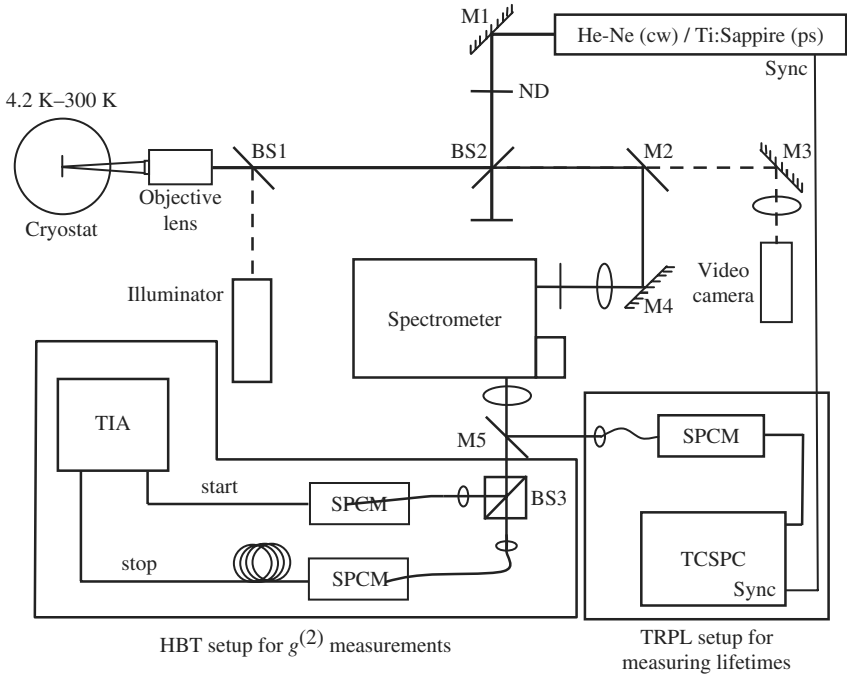

Figure 2. Optical arrangement for micro-PL, HBT ($g^{(2)}$) and TRPL measurements. A He:Ne laser or a picosecond laser (Ti:Sapphire Tsunami) delivers the laser light to the sample via mirror M1 and the objective lens. BS1 is a dichroic beamsplitter that reflects the pump light and transmits the photoluminescence. The photoluminescence is thus collected and returns along the same route to BS2 where it is directed through M2, M4 and focused onto the spectrometer slit. A 0.75 m double spectrometer (SPEX 1402) or a 0.55 m (TRIAX 550, Jobin Yvon) spectrometer is used to study spectra (with a charged coupled detector (CCD)) or to filter the light around the quantum dot emission. For $g^{(2)}$ measurements mirror M5 is flipped away and the light transmitted through the spectrometer is recollimated and passes through a 50:50 beamsplitter BS3, to two fibre-coupled single photon counting modules (SPCM). The photo-pulses are used as start and stop inputs to a time interval analyser (TIA). To measure dot lifetimes, the light transmitted through the spectrometer is again recollimated then reflected by mirror M5 and coupled into a fibre connected to the single photon counting module (SPCM) and photodetections are recorded using the time-correlated single photon counting (TCSPC) card. The sample is housed in an optical access cryostat under a 0.5 mm thick window. White light illumination can be used with a video camera to allow sample alignment when M2 is flipped away.

a maximum pulse energy of $\sim 1.2 \times 10^{-14}$ J per pulse. The laser wavelength was tuned to 808 nm and the laser beam was focused by a microscope objective lens (NA = 0.7) onto the sample with an effective spot size of $\sim 3\,\mu$m. The luminescence was collected by the same microscope objective and was sent to a 0.55 m monochromator with two outputs allowing connection to a liquid-nitrogen cooled CCD for μPL measurements or to a Hanbury Brown and Twiss (HBT) photon correlation apparatus, which measures the second-order intensity autocorrelation function ($g^{(2)}(\tau)$). The HBT set-up consists of a 50/50 non-polarizing beamsplitter, two fibre-coupled silicon

single photon counting modules (SPCMs) and a modulation domain analyser (HP53310A). To save measurement time, a passive time-out circuit was added between the start and stop inputs. Lifetime measurements were made using a modified Perkin Elmer SPCM [13, 14] with a timing resolution of ~400 ps (full width at half-maximum) in conjunction with a Becker and Hickl SPC600 time-correlated single photon counting (TCSPC) card with a timing resolution of 11 ps (full width at half-maximum).

4. Results

4.1 *Quality factors*

The efficiency of a single photon source based upon a single InAs quantum dot embedded within a planar GaAs layer is limited by the poor extraction efficiency of photons from the semiconductor. This efficiency can be improved dramatically by placing the dot within a microcavity [7, 8]. A suitable microcavity will modify the spontaneous emission of a dot on-resonance with the cavity mode, both increasing the spontaneous emission rate and improving the collection efficiency, thereby increasing the efficiency of the source. The decrease in lifetime of a quantum dot on-resonance with a cavity mode is characterized by the Purcell factor (P_F) [15]. To obtain a high P_F, microcavities with high Q factors and low modal volumes (V) are required ($P_F = (3Q/4\pi^2 V)(\lambda_c/n)^3$, where λ_c is the air wavelength of the cavity mode and n is the refractive index of the medium). The measured Q factors for small diameter microcavity pillars are plotted in figure 1. The measured Q factors of 12 000 for a 1.5 μm diameter pillar and 3000 for a diameter of 0.9 μm are amongst the highest reported for small diameter pillars (diameter <2 μm) [11]. From these measured Q factors, a maximum value of P_F in excess of 70 is calculated for a 1.5 μm diameter pillar.

For larger pillars (with diameter ≥2 μm) or planar microcavities, the wavelength of the fundamental cavity resonance is principally determined by the optical thickness of the cavity spacer. As the diameter is reduced until it approaches 1 μm (i.e. wavelength scale) the fundamental resonance is blue-shifted due to the increasing transverse component in the HE_{11} waveguide mode. This can be quantitatively understood by using approximate simulations, such as the transfer-matrix method coupled to a calculation of the waveguide modes using an average pillar refractive index. However for detailed estimates of the cavity Q, we used the 3D Finite Difference Time Domain (FDTD) simulation method. For the FDTD method [16], we place a broad band dipole source in the centre of the microcavity and apply a short excitation pulse to probe the mode spectrum. The cavity then rings at its resonant frequency and we monitor the cavity ringdown using a probe above the pillar. Taking the Fourier transform of the ringdown signal (in the time domain) allows us to determine the resonant frequencies of the waveguide cavity and also gives us an estimate of the Q factor ($Q = \lambda/\Delta\lambda$). We have calculated Q factors for various pillar diameters with the same cavity design as the pillars used in these

experiments (20 top mirror pairs and 27 bottom pairs). The simulation results and the experimental data are shown in figure 1.

The Q factors obtained from both experiment and FDTD simulations show the expected behaviour. The high Q factors found in large diameter micropillars are maintained down to a pillar diameter of 1–2 μm at which point the field intensity at the pillar edge becomes significant leading to increasing loss for smaller pillars and a corresponding reduction in Q factor [17]. Although the Q factors obtained from both measurement and simulations follow the same trend, the measured values are lower than the simulated ones, particularly for small pillars with diameter less than ~1.5 μm where the Q factors are being degraded due to surface imperfections not included in the FDTD simulations. This indicates that although the Q factors reported here are amongst the best reported for pillars of such small dimensions, the theoretical limit achievable in perfect pillars is yet to be reached.

4.2 *Polarized single dot emission*

A single photon source which emits photons with a defined polarization is important for many applications in quantum optics and quantum computation (where quantum indistinguishability is important) and in some implementations of quantum cryptography [18]. Such a polarized single photon source will be twice as efficient as using an unpolarized source in conjunction with a polarizer since using a polarizer involves rejection of half the emitted photons.

The high power μPL spectrum for an elliptical micropillar with major and minor axis 2.0 and 0.8 μm respectively, measured using the 633 nm, cw, HeNe laser, is shown in figure 3(*a*). Two cavity modes are shown with opposite linear polarizations. The lower energy mode is polarized with the E field parallel to the major axis of the ellipse (x-polarized) and the higher energy mode is polarized with the E field parallel to the minor axis of the ellipse (y-polarized). The emission of a quantum dot emitting off-resonance with a cavity mode is, in general, unpolarized. As the emission energy of the quantum dot is tuned by varying the temperature, the component of emission from the dot having the same polarization as the resonant mode is selectively enhanced. When the dot is on-resonance with the polarized cavity mode, the emission from the quantum dot can have a degree of linear polarization in excess of 0.9†; the degree of enhancement depending upon how well the quantum dot couples to the cavity.

Figure 3(*b*) shows the low power μPL spectrum from the pillar described above. The x-(y-)polarized emission spectrum is shown in black (grey). The spectra were measured at a temperature of 35 K where one quantum dot (labelled D) is on-resonance with the x-polarized cavity mode. It is clear that this dot is predominantly x-polarized in contrast to the other dots shown, which are not on-resonance with either cavity mode and are unpolarized. The high degree of polarization of this dot is due to the selective enhancement of the x-polarized PL emission when the dot

† Degree of polarization is defined as $[I(P_x) - I(P_y)]/[I(P_x) + I(P_y)]$, where $I(P_x)$ and $I(P_y)$ are the x- and y-polarized μPL intensities respectively.

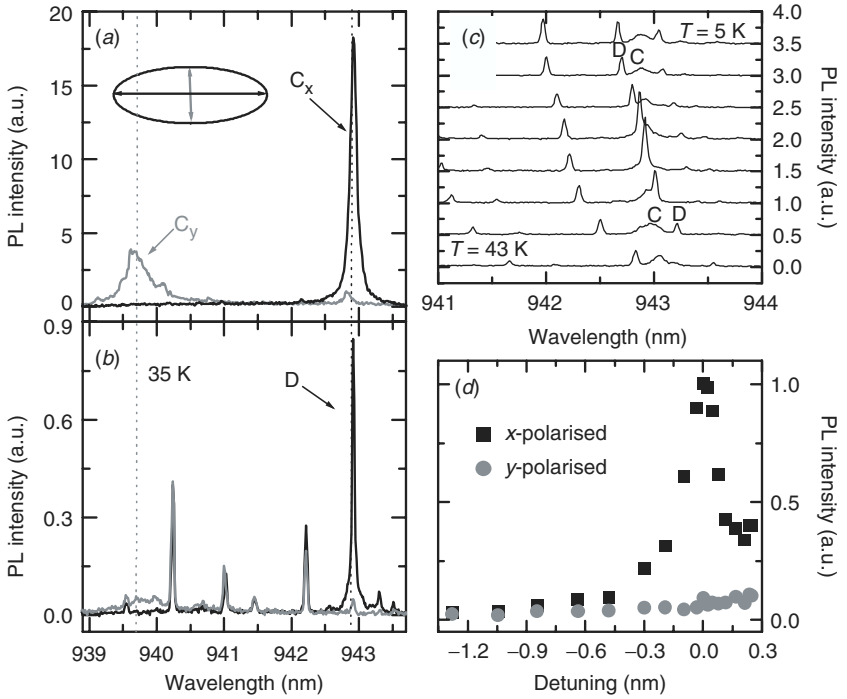

Figure 3. (*a*) High power μPL spectra from an elliptical micropillar with major and minor axes of 2.0 and 0.8 μm respectively. Emission polarized parallel to the major (*x*-polarized) and minor (*y*-polarized) axis of the ellipse is shown in black and grey respectively. (*b*) Low power μPL spectra from the same pillar measured at 35 K: *x*-(*y*-)polarized emission is shown in black (grey). A dot, D, is on-resonance with the *x*-polarized cavity mode and is highly polarized. (*c*) Low power *x*-polarized μPL spectra for the sample at temperatures between 5 and 43 K. As the temperature is varied the dot, D, moves into and out of resonance with the cavity mode C. (*d*) PL intensity of the *x*- and *y*-polarized components for dot D as a function of detuning from the cavity mode.

is on-resonance with the *x*-polarized cavity mode and not due to any intrinsic polarization of the dot. This is clearly shown in figure 3(*c*) which shows the *x*-polarized μPL spectra for this pillar at temperatures between 5 and 43 K. By varying the temperature, the dot (D) emission is tuned into and out of resonance with the cavity mode (C). A clear enhancement of the PL emission is observed when the dot is on-resonance with the cavity mode. This is emphasized in figure 3(*d*) which shows the intensity of both polarization components of the dot emission as a function of detuning from the cavity mode. The *x*-polarized component shows a clear peak on-resonance while the *y*-polarized emission shows only the small decrease in intensity associated with raising the sample temperature.

4.3 *Lifetimes and Purcell factors*

Figures 4(*a*) and (*b*) show the low power μPL spectra from a micropillar with elliptical cross-section where the major and minor axes are 1.5 and

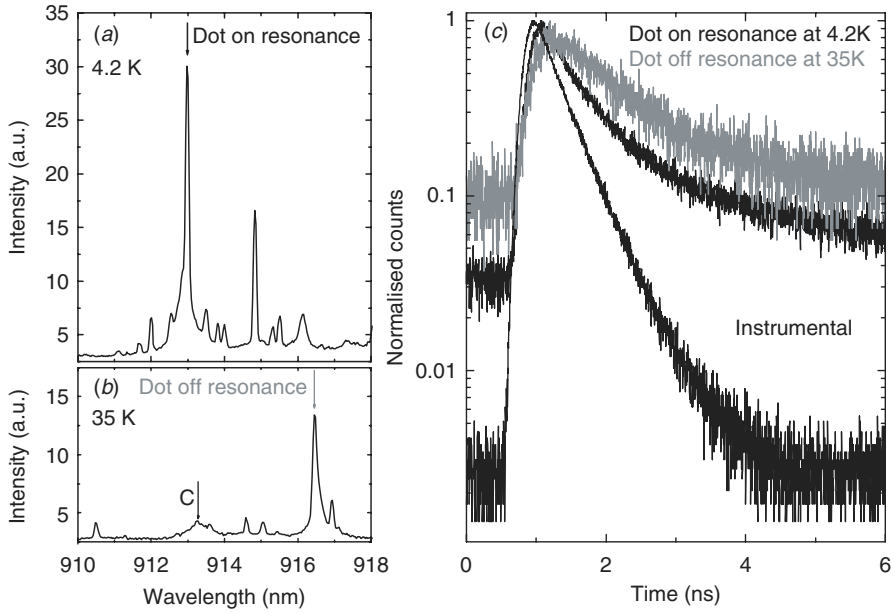

Figure 4. (*a*) μPL spectrum of an elliptical micropillar (major and minor axis 1.5 and 0.5 μm respectively) at a temperature of 4.2 K where a quantum dot is on-resonance with the cavity mode at a wavelength of 912.9 nm. (*b*) PL spectrum of the same pillar at a temperature of 35.0 K where the dot is off-resonance at 914.6 nm and the cavity mode C is at 913.3 nm. (*c*) TRPL measurements of the dot on-resonance at 4.2 K in black and off-resonance at 35 K in grey. The instrumental response of the system is also shown.

0.5 μm respectively. A pillar was selected that had a quantum dot emitting on resonance with the fundamental cavity mode at 4.2 K as shown in figure 4(*a*). This dot was moved off-resonance by raising the temperature to 35 K (figure 4(*b*)).

Figure 4(*c*), shows the normalized TRPL [19] traces taken when the dot is both on- and off-resonance at temperatures of 4.2 and 35 K respectively; an excitation wavelength of 811 nm and a repetition rate of 82 MHz was used to excite the pillar. The instrumental response of the system is shown for comparison. An exponential fit to the decays over the first few nanoseconds revealed that the quantum dot lifetime (τ) shortened from 1350 ps when the dot was off resonance with the cavity mode, to 550 ps when the dot was on-resonance, giving a measured Purcell factor of ~2.5. As noted by other groups [7, 20, 21], this measured Purcell enhancement is smaller than that calculated using the measured Q factor for this pillar, indicating non-optimal coupling between the cavity and the dot.

One issue arising from the use of the Ti:Sapphire laser was that its repetition frequency of 82 MHz was found to be too high and did not permit the dot emission to decay fully before the incidence of the next pulse. The effect of the laser repetition rate on the decay time was investigated by repeating the experiment using a semiconductor laser with a wavelength 784 nm, pulse width of 80 ps and a repetition frequency of 5 MHz. A comparison of the results is shown in figure 5. It is clear that the TRPL has

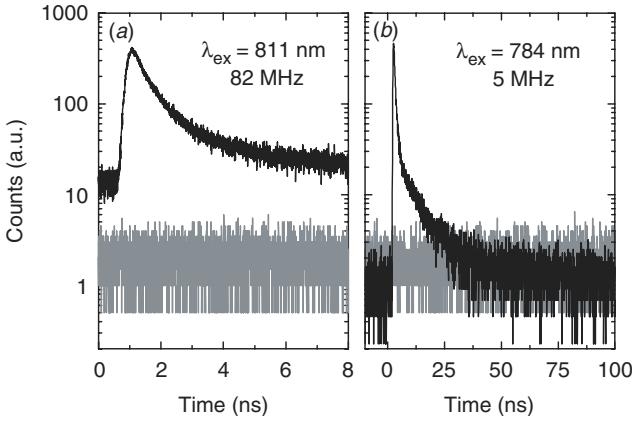

Figure 5. Comparison of TRPL traces of a quantum dot on resonance with the cavity mode at a temperature of 5 K obtained using different repetition rate lasers. The background signal measured with no laser excitation is shown for comparison in grey. (*a*) TRPL trace obtained using an excitation wavelength of 811 nm, repetition frequency of 82 MHz and period of 12.2 ns. (*b*) TRPL trace obtained using an excitation wavelength or 784 nm, repetition frequency of 5 MHz and period of 200 ns. The time $t = 0$ is set by the timing electronics. Note that the decay at 82 MHz does not reach the background level, while it does reach the background level when a frequency of 5 MHz is used.

not fully decayed to the background count level in the 82 MHz repetition rate case, whilst the signal has fully decayed in the lower repetition frequency excitation measurement. This indicates the presence of a long-lived component in the luminescence decay with a lifetime $\tau \sim 10$–40 ns depending upon the excitation conditions. Exponential fits to the TRPL data obtained using the 784 nm, 5 MHz excitation laser did not show as significant a reduction in lifetime as the dot was moved on-resonance. Further studies are in progress to determine the optimum excitation conditions for this type of measurement. However it is clear that a combination of low excitation frequency and close-to-resonant photon energy will be required.

4.4 *Single photon generation in circular and elliptical pillars*

Single QD emission can be isolated in small diameter micropillars (<4 μm) under low pump power (inset to figure 6(*b*)), and can be tuned on- and off-resonance with the cavity mode by varying temperature. At higher excitation powers, the cavity mode dominates with single QD emissions washed out. In this subsection we report single photon generation in circular pillars and polarized single photon generation in elliptical pillars.

Single photon generation was examined by measuring the second-order intensity autocorrelation function ($g^{(2)}(\tau)$) using the HBT arrangement shown in figure 2. $g^{(2)}(\tau)$ is defined as

$$g^{(2)}(\tau) = \frac{\langle n(t)n(t+\tau)\rangle}{\langle n\rangle^2} = \frac{p(t : t+\tau)}{p(t)},$$

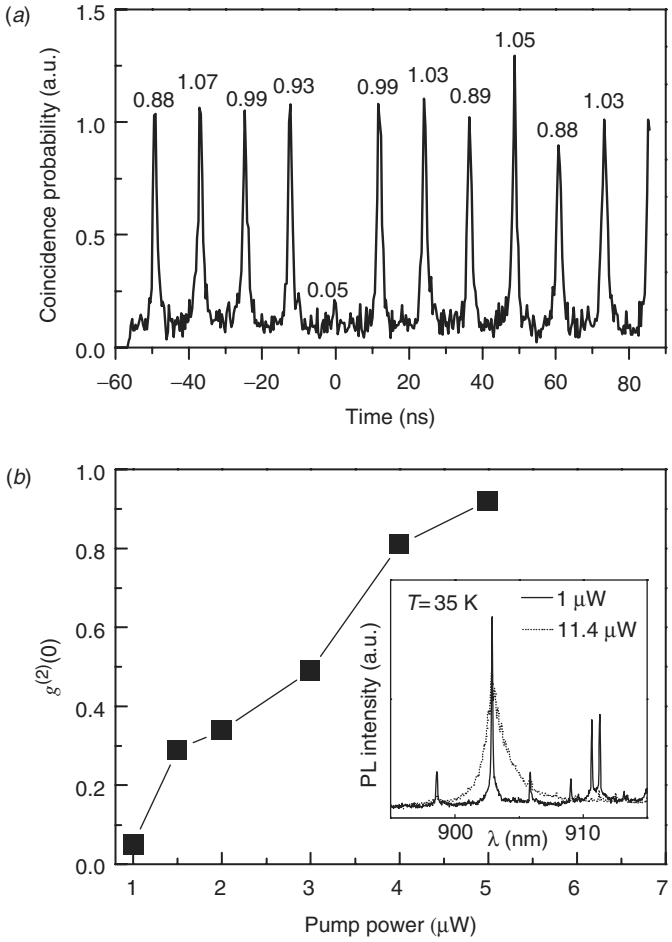

Figure 6. (*a*) Measured second-order correlation function for emission from the quantum dot on resonance with the cavity as shown in the inset to figure 6(*b*). The multi-photon probability is very low. (*b*) The power dependence of $g^2(0)$. Inset, PL spectrum of a quantum dot on resonance with the cavity mode of a circular micropillar of diameter 600 nm excited at $\lambda = 810$ nm and power $P = 1\,\mu$W (black line) and 11.4 μW (dotted line).

where $n(t)$ is the photocount probability at time t and the angular brackets denote ensemble averages. This can also be cast in terms of the conditional probability of recording photodetections at times t and $t+\tau$, $p(t : t+\tau)$ normalized by the probability for recording a single detection $p(t)$. At low count rates the time interval analyser (TIA) measures the probability that a stop pulse at delay time τ follows the start pulse; this probability is proportional to $p(t : t+\tau)$, allowing us to estimate $g^{(2)}(\tau = 0)$ after normalization. Of course, in this set-up there were two detectors viewing the same source through the beamsplitter as a single detector cannot measure a second photo-pulse arriving during the detector dead time after the first pulse. However this still provides a good estimate of $g^{(2)}(\tau)$. Also in the case of pulsed

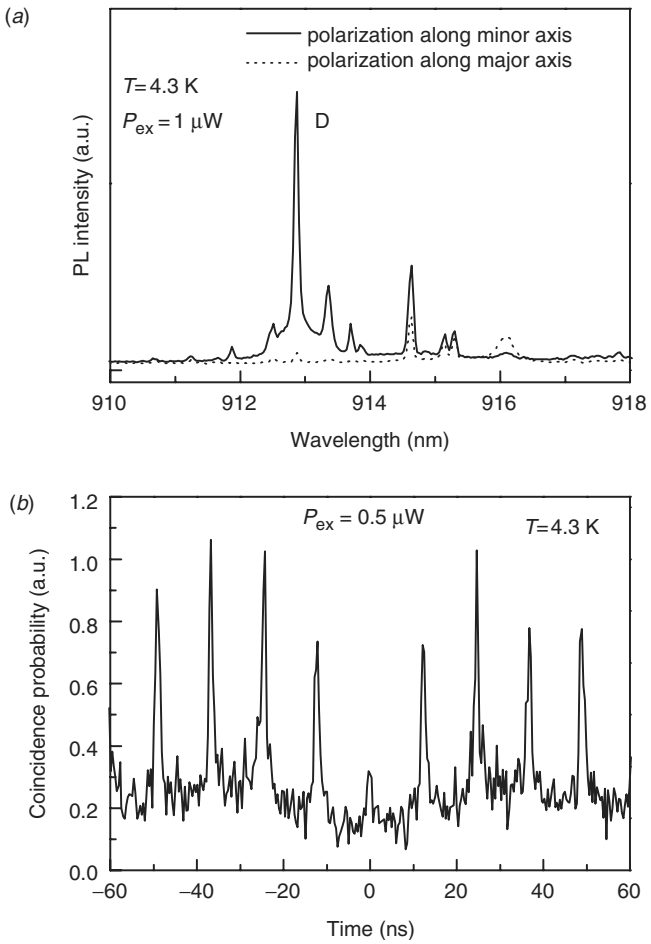

Figure 7. (*a*) Spectrum showing the emission from an elliptical micropillar with major and minor axes 1.5 and 0.5 μm respectively. The emission polarized parallel to the major (dashed line) and minor axis (solid line) is shown. A quantum dot (D) is on resonance with the cavity mode at 912.9 nm. (*b*) $g^{(2)}(\tau)$ of the emission from the quantum dot labelled (D) in (*a*).

pumping we will record a set of peaks in the time interval plot due to the fact that the probability of stops falling outside the pump pulses is low. For ideal single photon sources, the peak at zero time delay should disappear completely, representing a probability of zero for a multi-photon event [3, 6, 22].

In a circular pillar with diameter of 0.6 μm, we observed a rather weak central coincidence peak (figure 6(*a*)). The normalized area of the central peak was calculated using a Lorentzian fitting and gave $g^{(2)}(\tau = 0) = 0.05$, indicating that multi-photon emission is suppressed by a factor of at least 20. With increasing pump power, the single QD emission saturates and the cavity mode intensity develops rapidly. As a result, $g^{(2)}(\tau = 0)$ increases rapidly with the pump power (as shown in figure 6(*b*)).

Progressing from circular pillars to elliptical pillars, the two-fold degenerate cavity is split into two modes: one polarized along the major axis (x-polarized) and another polarized along the minor axis (y-polarized) as discussed in section 4.2. In an elliptical pillar with a major axis of 1.5 μm and a minor axis of 0.5 μm, we observe a QD on resonance with the cavity mode at 912.9 nm, polarized along the minor axis (figure 7(*a*)). The polarized single photon generation is verified by observation of a weaker central coincidence peak with $g^2 \leq 0.3$ (figure 7(*b*)) [10, 22].

5. Conclusions

Semiconductor microcavity pillars are shown to provide the basis for efficient sources of single photons, both polarized and unpolarized. A Purcell reduction of the lifetime of a quantum dot when on-resonance with a cavity mode of ~2.5 has been demonstrated. The multiphoton emission probability from a circular micropillar is shown to be reduced by a factor of 20, while that of a quantum dot within an elliptical microcavity is also shown to be reduced, but by a smaller factor. It has been demonstrated that the use of elliptical micropillars allows the polarization of the emitted photon to be controlled. All of these features demonstrate the excellent potential of quantum dot micropillar sources in quantum information processing applications.

Acknowledgements

The authors would like to acknowledge the support of EPSRC and MOD/DSTL through the Joint Research Grants Scheme ref. no. Dstl/GR/T09408, support from QIP IRC (GR/S822176) and EU IP:015848 QAP and use of Edinburgh Instruments Ltd, Analytical T900 Software V6.0.

References

[1] D.J. Mowbray and M.S. Skolnick, J. Phys. D Appl. Phys. **38** 2059 (2005).
[2] S. Benjamin, Science **290** 2273 (2000).
[3] B. Lounis and W.E. Moerner, Nature **407** 491 (2000).
[4] C. Kurtsiefer, S. Mayer, P. Zarda, *et al*., Phys. Rev. Lett. **85** 290 (2000).
[5] P. Michler, A. Imamoglu, M.D. Mason, *et al*., Nature **406** 968 (2000).
[6] C. Santori, M. Pelton, G. Solomon, *et al*., Phys. Rev. Lett. **86** 1502 (2001).
[7] J.M. Gerard, B. Sermage, B. Gayral, *et al*., Phys. Rev. Lett. **81** 1110 (1998).
[8] G.S. Solomon, M. Pelton and Y. Yamomoto, Phys. Rev. Lett. **86** 3903 (2001).
[9] B. Gayral, J.M. Gerard, B. Legrand, *et al*., Appl. Phys. Lett. **72** 1421 (1998).
[10] D.C. Unitt, A.J. Bennett, P. Atkinson, *et al*., Phys. Rev. B **72** 033318 (2005).
[11] A. Daraei, A. Tahraoui, D. Sanvitto, *et al*., Appl. Phys. Lett. **88** 051113 (2006).
[12] D. Englund, D. Fattal, E. Waks, *et al*., Phys. Rev. Lett. **95** 013904 (2005).
[13] I. Rech, I. Labanca, M. Ghioni, *et al*., Rev. Sci. Instrum. **77** 033104 (2006).
[14] K.J. Gordon, V. Fernandez, G.S. Buller, *et al*., Opt. Express **13** 3015 (2005).
[15] E.M. Purcell, Phys. Rev. **69** 681 (1946).

[16] Y.-L.D. Ho, T. Cao, P.S. Ivanov, *et al.*, Int. J. Quantum Informat. **3** 229 (2005).
[17] D. Sanvitto, A. Daraei, A. Tahraoui, *et al.*, Appl. Phys. Lett. **86** 19, 1109 (2005).
[18] N. Gisin, G. Ribordy, W. Tittel, *et al.*, Rev. Mod. Phys. **74** 145 (2002).
[19] J.M. Smith, P.A. Hiskett, I. Gontijo, *et al.*, Rev. Sci. Instrum. **72** 2325 (2001).
[20] C. Santori, D. Fattal, J. Vuckovic, *et al.*, New J. Phys. **6** 89 (2004).
[21] A.J. Bennett, D.C. Unitt, P. Atkinson, *et al.*, Opt. Express **50** 5759 (2004).
[22] E. Moreau, I. Robert, J.M. Gerard, *et al.*, Appl. Phys. Lett. **79** 2865 (2001).